Journal of Geriatric Cardiology | JGC
RESEARCH ARTICLE
J Geriatr Cardiol 2024; 21(9): 899–912

Aldo-Keto reductase 1C3 reduces myocardial cell damage after acute myocardial infarction by activating the Kelch-like ECH-associated protein 1-nuclear factor erythroid 2-related factor 2-antioxidant response element pathway to inhibit ferroptosis

Wang MIAO[1,2], Yun-Zhao HU[1,2,✉]

1. Department of Cardiology, Shunde Hospital, Southern Medical University, the First People's Hospital of Shunde, Foshan, China; 2. The Second School of Clinical Medicine, Southern Medical University, Guangzhou, China
✉ Correspondence to: doctorxnk@163.com
https://doi.org/10.26599/1671-5411.2024.09.001

ABSTRACT

Background Acute myocardial infarction (AMI) is a high-risk cardiovascular condition associated with increased cellular damage and oxidative stress. Aldo-Keto Reductase 1C3 (AKR1C3) is a stress-regulating gene. Nevertheless, its specific role and mechanisms regarding AMI remain unclear.

Methods We assessed cardiac function through echocardiography; tissue damage was evaluated using Hematoxylin and Eosin (HE) and Masson trichrome staining. AKR1C3 expression levels were measured through Reverse transcription-quantitative polymerase chain reaction and western blot. Assessed cell viability using Cell Counting Kit-8 and lactate dehydrogenase (LDH) assays. The extent of ferroptosis was determined by measuring the levels of Fe^{2+}, boron-dipyrromethane (BODIPY) and malondialdehyde (MDA), the glutathione/glutathione disulfide (GSH/GSSG) ratio, and the expression of Glutathione Peroxidase 4 (GPX4) and Solute carrier 7A11 (SLC7A11). Kelch-like ECH-associated protein 1-Nuclear factor erythroid 2-related factor 2-Antioxidant response element (Keap1-Nrf2-ARE) pathway activation was analyzed through western blotting. Nrf2 was inhibited with ML385 and activated with (R)-Sulforaphane to investigate the Keap1-Nrf2-ARE pathway.

Results The rats in the AMI group displayed reduced heart function, more tissue damage, and lower AKR1C3 expression compared to the Sham group. Similarly, hypoxia-treated H9C2 cells showed reduced viability, and decreased AKR1C3 expression. Overexpressing AKR1C3 in H9C2 cells enhanced viability. Knocking down AKR1C3 exhibited the opposite effect. Of the inhibitors tested, Ferrostatin-1 most effectively restored cell viability in hypoxia-treated H9C2 cells. Moreover, H9C2 cells subjected to hypoxia suggested Keap1-Nrf2-ARE pathway inhibition. Overexpressing AKR1C3 reduced ferroptosis and activated the Keap1-Nrf2-ARE pathway in hypoxia-treated cells, knocking down AKR1C3 exhibited the opposite effect. Further experiments using ML385 in hypoxia-treated H9C2 cells with overexpressed AKR1C3 showed decreased viability and increased ferroptosis compared to the control. Using (R)-Sulforaphane in hypoxia-treated H9C2 cells with knocked-down AKR1C3 exhibited the opposite effect.

Conclusion This study's findings indicate that AKR1C3 plays a role in regulating ferroptosis in myocardial cells, with the Keap1-Nrf2-ARE pathway likely being a key mechanism behind it.

Acute myocardial infarction (AMI) is a significant disease that impacts human health and contributes to increased socioeconomic burden.[1,2] Emergency percutaneous coronary intervention (PCI) and other revascularization methods have saved many lives. However, the prognosis for patients with AMI often remains poor.[3] While the pathophysiological changes in AMI arise from a complex interplay of mechanisms, myocardial cell damage is a central factor.[4] Multiple stud-

ies suggest that reducing myocardial cell damage after AMI is crucial to improving patient outcomes.[5,6]

Oxidative stress is a major cause of myocardial cell damage following AMI.[7] Regulating oxidative stress is an effective strategy to limit this damage.[8] As a stress-regulating gene, Aldo-Keto reductase 1C3 (AKR1C3) plays a pivotal role in cell damage and response to oxidative stress.[9] Huang, *et al.*[10] found that the interaction between AKR1C3 and β-catenin was an essential mechanism in reducing oxidative stress in PC12 cells. Alternatively, Liang, *et al.*[11] suggested that AKR1C3 might be a potential biomarker for AMI. Despite this, the detailed molecular mechanisms behind the role of AKR1C3 in AMI remain unclear.

Ferroptosis, a form of cell death closely linked to oxidative stress,[12] plays a significant role in AMI progression.[13,14] Jiang, *et al.*[15] suggested that the loss of the hematopoietic progenitor Kinase interacting protein-55 (HIP-55) gene after AMI increases myocardial cell ferroptosis and heart damage, while cardiac-specific overexpression of HIP-55 significantly alleviated these effects. Similarly, Yu, *et al.*[16] reported that Epigallocatechin gallate alleviated myocardial cell ischemic injury by reducing ferroptosis after AMI.

Cells respond to oxidative stress by activating a series of protective mechanisms against endogenous and exogenous damage. The Kelch-like ECH-associated protein 1-Nuclear factor erythroid 2-related factor 2-Antioxidant response element (Keap1-Nrf2-ARE) pathway is a critical player in these anti-damage responses.[17] The binding pattern between Keap1 and Nrf2 varies depending on the cell environment and directly determines ARE expression in the cell nucleus, leading to different biological outcomes.[18,19] Liu, *et al.*[20] demonstrated that hyperbaric oxygen preconditioning protected against cardiac damage in rats with AMI, with the effect attributed to the Keap1-Nrf2-Heme oxygenase 1 (Ho1) antioxidant defense system. In a separate study, Ma, *et al.*[21] found that miR-200a levels were down-regulated in the myocardial tissue of mice with AMI, while miR-200a overexpression decreased myocardial cell apoptosis by regulating the Keap1-Nrf2 and β-catenin pathways.

In this study, a rat AMI model was established by coronary artery ligation. H9C2 cells were subjected to hypoxia to simulate in vitro conditions. The study subsequently examined the impact of AKR1C3 on myocardial cell viability and ferroptosis, with a particular focus on the role of the Keap1-Nrf2-ARE pathway.

METHODS

Experimental Animals and Ethics

Sprague Dawley rats (200-250g), regardless of gender, were used for this study. They were kept in an environment with a humidity of 60%, a temperature of 23°C, and alternating light-dark cycles. The rats had unrestricted access to food and water. The Ethics Committee of the Shunde Hospital of Southern Medical University approved the experimental protocols in accordance with the Guide for the Care and Use of Laboratory Animals by the National Institutes of Health.

Establishment of the AMI Model

The rats were anesthetized using a veterinary anesthesia machine for small animals (RWD Life Science, China) and then placed on a heating pad (37°C) in a supine position. They were intubated for tracheal ventilation and connected to a small animal ventilator (Kewbasis, China), with a tidal volume of 3.5 mL, a 1: 2 inspiratory-to-expiratory ratio, and a ventilation rate of 80 breaths/min. A mixture of 2/3 air, 1/3 oxygen, and isoflurane was used during the procedure. After this, the rats' chest hair was shaved and a thoracotomy was performed between the fourth and fifth ribs, where the heart pulsation was most apparent. Soft tissues were separated layer by layer to expose the ribs, which were then spread open to access the heart. The pericardium was cut, and the left coronary artery was litigated 1.5 mm from the apex of the left atrial appendage near the pulmonary artery conus using a 6-0 suture. Once coronary artery occlusion (i.e., the distal myocardium turned pale when the suture was tightened) was confirmed by visual observation, the thoracic cavity was closed in layers. After that, the rats were removed from the ventilator and closely monitored as they recovered consciousness until regaining mobility. The Sham group underwent the same surgical procedure, except the suture under the left coronary artery was not tied.

Ultrasound Examination

After the rats were anesthetized with 2% isoflurane, heart images were acquired using a Vevo2100 ultrasound system (VisualSonics, USA) equipped with a 24 MHz probe.

Infarct Area Measurement

We rapidly extracted the hearts 24 h after inducing myocardial infarction. The hearts were frozen at -20°C for 30 min before they were sliced into 2 mm thick sections. Subsequently, following the manufacturer's instructions, the slices were incubated in 2% Triphenyl Tetrazolium Chloride (TTC) solution (Solarbio, China) at 37°C for 15 min, and then dried and fixed in 4% paraformaldehyde solution for 24 h before being photographed.

Pathological Staining

The heart tissue was fixed in 4% paraformaldehyde overnight, embedded in paraffin, and sectioned into 4 μm slices. After deparaffinization, Hematoxylin and Eosin (HE) and Masson staining were performed according to the manufacturer's instructions (Servicebio, China).

Cell Culture and Treatment

Rat myocardial cells (H9C2), obtained from the American Type Culture Collection), were cultured in Dulbecco's Modified Eagle Medium (Gibco, USA) supplemented with 10% fetal bovine serum (Newzerum, New Zealand), 100 IU/mL penicillin, and 100 mg/mL streptomycin (Gibco, USA). The cells were incubated at 37°C in a humidified atmosphere with 5% CO_2. When cell confluence reached 80%, they were either passaged or subjected to hypoxic treatment. In contrast, the control group received no additional treatment. All cells were harvested 12 h after incubation.

Cell Viability Assay

Cell viability was assessed using a Cell Counting Kit (CCK)-8 assay kit (Beyotime, China) following the manufacturer's instructions. The obtained CCK-8 readings were then converted into cell viability.

Lactate Dehydrogenase Release Assay

The Lactate dehydrogenase (LDH) level in the culture medium's supernatant was measured using an LDH assay kit (DOJINDO, Japan) following the manufacturer's instructions.

Fe^{2+} Detection

Following the manufacturer's instruction, H9C2 were first cultured in six-well plates, When cell confluence reached 80%, they were either normoxia or subjected to hypoxic treatment,Then, the cells were treated with 1 μM FerroOrange probe (DOJINDO, Japan) working solution at 37°C for 30 min. Then, the reaction mixture was added 400 μL Hanks' Balanced Salt Solution (HBSS), The levels of Fe^{2+} were measured by flow cytometry (BD, USA).

Boron-dipyrromethene Assay

Following the manufacturer's instruction, H9C2 were either normoxia or subjected to hypoxic treatment. Then, the cells were treated with 5 μM Boron dipyrromethene (BODIPY) (Gibco, USA) working solution at 37°C for 30 min. Then, the reaction mixture was added 400 μL HBSS. The levels of BODIPY were measured by flow cytometry (BD, USA).

Western Blot

Total protein was extracted from rat myocardial tissue or H9C2 cells using Radioimmunoprecipitation Assay buffer (Beyotime, China). Subsequently, nuclear and cytoplasmic proteins were isolated using a nuclear and cytoplasmic protein extraction kit (Beyotime, China). Following ultrasonication and high-speed centrifugation, the supernatant containing the protein extracts was collected. Protein concentrations were determined using a Bicinchoninic acid protein assay kit (Gibco, USA). Samples containing 25 μg of protein were denatured, separated by electrophoresis, and transferred onto a polyvinylidene fluoride membrane (Millipore, Germany). The membrane was blocked with Tris-Buffered saline with Tween (TBST) containing 5% non-fat milk for 1 hour at room temperature, followed by overnight incubation with primary antibodies at 4°C. Primary antibodies included anti-AKR1C3 from GeneTex (USA), along with anti-solute carrier 7A11 (SLC7A11), anti-Glutathione peroxidase 4 (GPX4), anti-Keap1, anti-Nrf2, anti-HO-1, anti-Nicotinamide adenine dinucleotide phosphate dehydrogenase Quinone dehydrogenase (NQO-1), anti-α-

Tubulin, anti-β-Actin, and anti-LaminB1 from Proteintech (China). After washing the membrane with TBST, it was incubated with Horseradish Peroxidase-conjugated secondary antibodies for 1 h at room temperature. Following a final wash, protein bands were visualized via chemiluminescence (BIO-RAD, USA). Western blots were performed at least three times, and the results were quantified using ImageJ software.

Reverse transcription-Quantitative Polymerase Chain Reaction

Total RNA was extracted from rat myocardial tissue or H9C2 cells using an RNA extraction kit (Mabio, China) as per the manufacturer's instructions. The isolated RNA was reverse transcribed into cDNA with a reverse transcriptase (Vazyme, China). Subsequently, reverse transcription-quantitative polymerase chain reaction (RT-qPCR) was performed using a SYBR Green RT-PCR kit (Vazyme, China). The RT-qPCR procedure involved initial denaturation at 95°C for 30 s, followed by 40 cycles of 95°C for 10 s and another 40 cycles of 60°C for 30 s, ending with a melt curve analysis. Relative mRNA expression levels were then normalized to β-actin and evaluated using the $2^{-\Delta\Delta Ct}$ method. The primer sequences are provided in Table 1.

Lentiviral Transfection

H9C2 cells were seeded in 6-well plates and grown to about 50%–70% confluence. On the transfection day, the cells were exposed to either the interference or the control virus. After a 24-h incubation, the culture medium was replaced with a fresh medium. The overexpression group and its control group were labeled with an Enhanced Green Fluorescent Protein (EGFP) fluorescent tag, allowing for transfection verification through fluorescence microscopy. Conversely, since the knockdown group and its control group had drug resistance, puromycin (1 μg/mL) was used for selection after transfection. Subsequently, RT-qPCR and western blotting were conducted to validate the transfection outcomes.

Statistical Analysis

All statistical analyses were carried out using GraphPad Prism 9.0 (GraphPad Software, La Jolla, CA, USA). Quantitative data were expressed as mean ± SD. A two-tailed student's *t*-test was used for comparisons between two groups, and a one-way analysis of variance was used for comparisons among multiple groups. $P < 0.05$ was considered statistically significant.

RESULTS

AKR1C3 Levels Decrease in the Myocardial Tissue of Rats with AMI

In this study, a rat AMI model was established to investigate the pathological changes after inducing AMI. As shown in Figures 1A-D, the AMI group exhibited a lower ejection fraction compared to the Sham group, with pronounced pale areas in TTC staining. HE staining revealed disorganized myocardial cell structures, extracellular matrix degradation, and capillary dilation. Masson trichrome staining indicated a notable increase in myocardial fibrosis. AKR1C3 levels in myocardial tissue were measured using RT-qPCR and western blot to characterize the changes in AKR1C3 after AMI. The results showed that AKR1C3 levels were significantly reduced in the AMI group compared to the Sham group (Figures 1E-G).

AKR1C3 Levels Decrease in Hypoxia-Treated H9C2 Cells

H9C2 cells were subjected to hypoxia to establish an in vitro AMI model. The results indicated that hypoxia-treated cells exhibited lower viability (Figure 2A) and higher levels of LDH release (Figure 2B) compared to the control group. Subsequently, changes in AKR1C3 in hypoxia-treated H9C2 cells were examined, revealing that mRNA and protein levels of AKR1C3 were significantly lower in the hypoxia-treated group than in the control group

Table 1 Primer sequences.

Gene Name	Forward Primer (5′—3′)	Reverse Primer (5′—3′)
AKR1C3	TGAGGAGAGAATCAGAGAGA	TCAGAGAATGGAAAGTTAGG
β-actin	TCAGGTCATCACTATCGGCAAT	AAAGAAAGGGTGTAAAACGCA

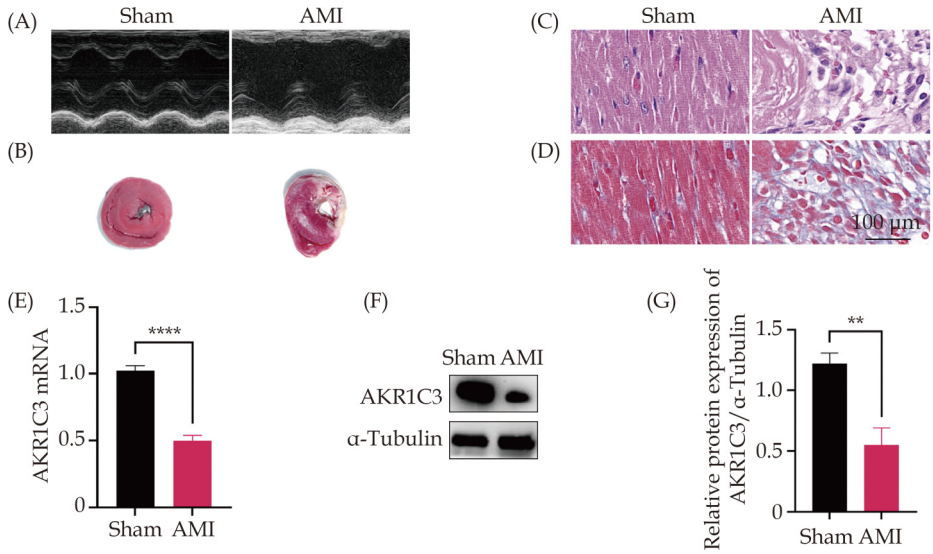

Figure 1 Rats with AMI exhibit decreased ejection fraction and significant tissue damage, along with reduced AKR1C3 levels in myocardial tissue. Comparison of the AMI and Sham groups for (A-D): Echocardiography, TTC staining, HE staining, and Masson trichrome staining; (E-G): mRNA and protein levels of AKR1C3 in myocardial tissue. $^{**}P < 0.01$, $^{****}P < 0.0001$. AMI: acute myocardial infarction; AKR1C3: Aldo-Keto reductase 1C3; HE: Hematoxylin and Eosin; TTC: triphenyl tetrazolium chloride.

(Figure 2C-E). These results align with those observed in the AMI rat model.

AKR1C3 Regulates H9C2 Cell Viability

Stable cell lines were developed with overexpressed or knocked-down AKR1C3 to investigate the role of AKR1C3 in hypoxia-treated H9C2 cells. The effectiveness of AKR1C3 manipulation was confirmed through RT-qPCR and Western blot (Figure 3A-C, F-H). Subsequent CCK-8 assay results indicated that H9C2 cells with overexpressed AKR1C3 showed higher viability and lower LDH release after hypoxia compared to the control group (Figure 3D, E). Conversely, H9C2 cells with knocked-down AKR1C3 exhibited the opposite effects (Figure 3I, J).

After Hypoxia, ferroptosis Is Increased, and the Keap1-Nrf2-ARE Pathway Is Inhibited in H9C2 Cells

We investigated different types of cell death to explore the forms of cell damage associated with reduced cell viability in hypoxia-treated H9C2 cells. We evaluated how various inhibitors affected cell viability under hypoxic conditions, including apoptosis inhibitor Z-VAD-FMK, necroptosis inhibitor Necrostatin-1, autophagy inhibitor 3-Methyladenine, and ferroptosis inhibitor Ferrostatin-1. The non-intervention group was given equivalent amounts of dimethyl sulfoxide as a control. As shown in Figure 4A, using different inhibitors led to varying degrees of change in cell viability, with Ferrostatin-1 exhibiting the most substantial recovery effect, suggesting that ferroptosis is likely the predominant form of cell death in hypoxia-treated H9C2 cells. We set up four groups to investigate ferroptosis in hypoxia-treated H9C2 cells further: Normoxia, Normoxia_Ferrostatin-1, Hypoxia, and Hypoxia_Ferrostatin-1 groups. The results indicated that when subjected to hypoxia treatment, H9C2 cells showed escalated levels of Fe^{2+}, BODIPY, and malondialdehyde (MDA) (Figure 4B-D), while the Glutathione/Glutathione disulfide (GSH/GSSG) ratio decreased. In addition, the western blot revealed reduced expressions of GPX4 and SLC7A11 after hypoxia (Figure 4E-H). Significantly, these effects, indicative of lipid peroxidation, could be partially reversed by Ferrostatin-1. These findings suggest that ferroptosis increases in hypoxia-treated H9C2 cells.

Research has shown that the Keap1-Nrf2-ARE pathway plays an essential role in the oxidative stress response[22] and AMI. We examined Keap1-Nrf2-ARE pathway expression in hypoxia-treated H9C2 cells to elucidate further how AKR1C3 regulates ferroptosis. Western blot showed that hypoxia-treated cells showed an increase in cytoplasmic Nrf2 and a decrease in nuclear Nrf2, along with higher Keap1 levels and lower levels of HO-1 and NQO-1

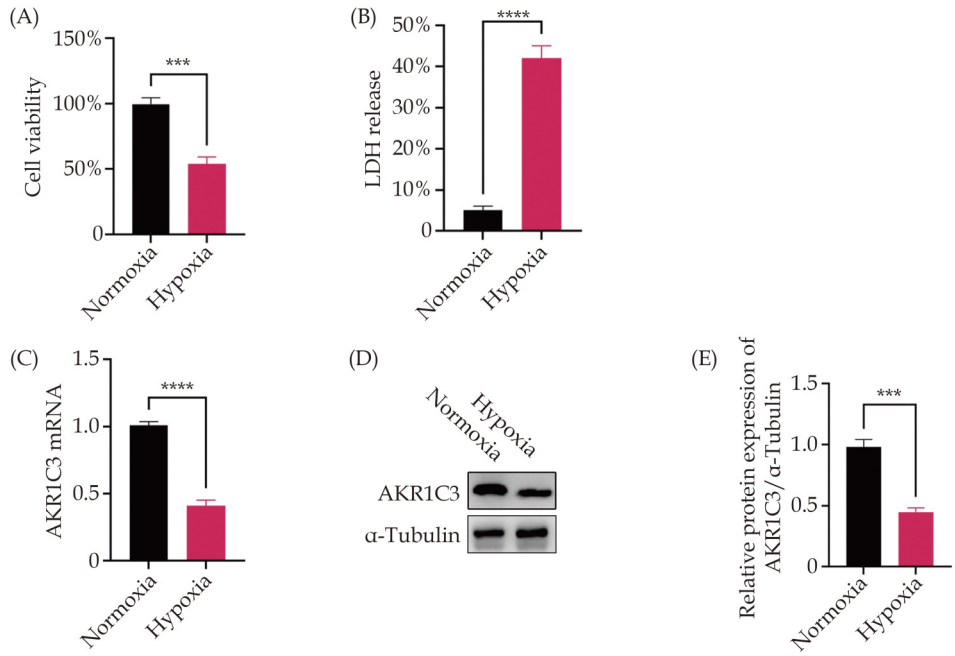

Figure 2 AKR1C3 levels decrease in hypoxia-treated H9C2 cells. For hypoxia-treated H9C2 cells. (A, B): Cell viability and LDH release; (C-E): mRNA and protein levels of AKR1C3. $^{***}P < 0.001$, $^{****}P < 0.0001$. AKR1C3: Aldo-Keto reductase 1C3; LDH: lactate dehydrogenase.

compared to the control group (Figure 4H, I). These results indicate that in hypoxia-treated H9C2 cells, the increase in ferroptosis stems from the inhibition of the Keap1-Nrf2-ARE pathway.

Ferroptosis Increases and the Keap1-Nrf2-ARE Pathway Is Inhibited in Rat Myocardial Tissue After AMI

In this section, the AMI rat model was investigated. The AMI group exhibited elevated MDA levels and a reduced GSH/GSSG ratio in myocardial tissue compared to the sham group (Figure 5A, B). In addition, the western blot indicated decreased levels of GPX4 and SLC7A11 (Figure 5C, D), suggesting that ferroptosis increased in rats after AMI. Regarding pathway regulation, rats in the AMI group showed increased cytoplasmic Nrf2 and decreased nuclear Nrf2 levels, along with increased total Keap1 levels and reduced HO-1 and NQO-1 levels. These findings indicate that the Keap1-Nrf2-ARE pathway is suppressed in rat myocardial tissue after AMI (Figure 5E, F).

AKR1C3 Regulates Ferroptosis and the Keap1-Nrf2-ARE Pathway in Hypoxia-Treated H9C2 Cells

We investigated the effects of AKR1C3 overexpression to explore further the role of AKR1C3 in regulating ferroptosis and the Keap1-Nrf2-ARE pathway in hypoxia-treated H9C2 cells. According to the results, the overexpressed (OE)_AKR1C3_Hypoxia group showed lower levels of Fe^{2+}, BODIPY, and MDA compared to the EGFP_Hypoxia group, while the GSH/GSSG ratio and expressions of GPX4 and SLC7A11 were elevated. These markers showed partial recovery with the introduction of Ferrostatin-1 (Figure 6A-F). This indicates that overexpressing AKR1C3 inhibits ferroptosis in hypoxia-treated H9C2 cells. Regarding pathway regulation, the OE_AKR1C3_Hypoxia group had increased nuclear and decreased cytoplasmic Nrf2 levels, along with lower total Keap1 and higher HO-1 and NQO-1 levels, suggesting activated Keap1-Nrf2-ARE pathway (Figure 6G-H).

In addition, hypoxia-treated H9C2 cells with AKR1C3 knockdown showed higher levels of Fe^{2+}, BODIPY, and MDA, lower GSH/GSSG ratios, and reduced GPX4 and SLC7A11 expressions compared to the control group. These levels partially recovered after introducing Ferrostatin-1, indicating that knocking down AKR1C3 promotes ferroptosis in hypoxia-treated H9C2 cells (Figure 6I-N). Regarding pathway regulation, the shAKR1C3_Hyp-

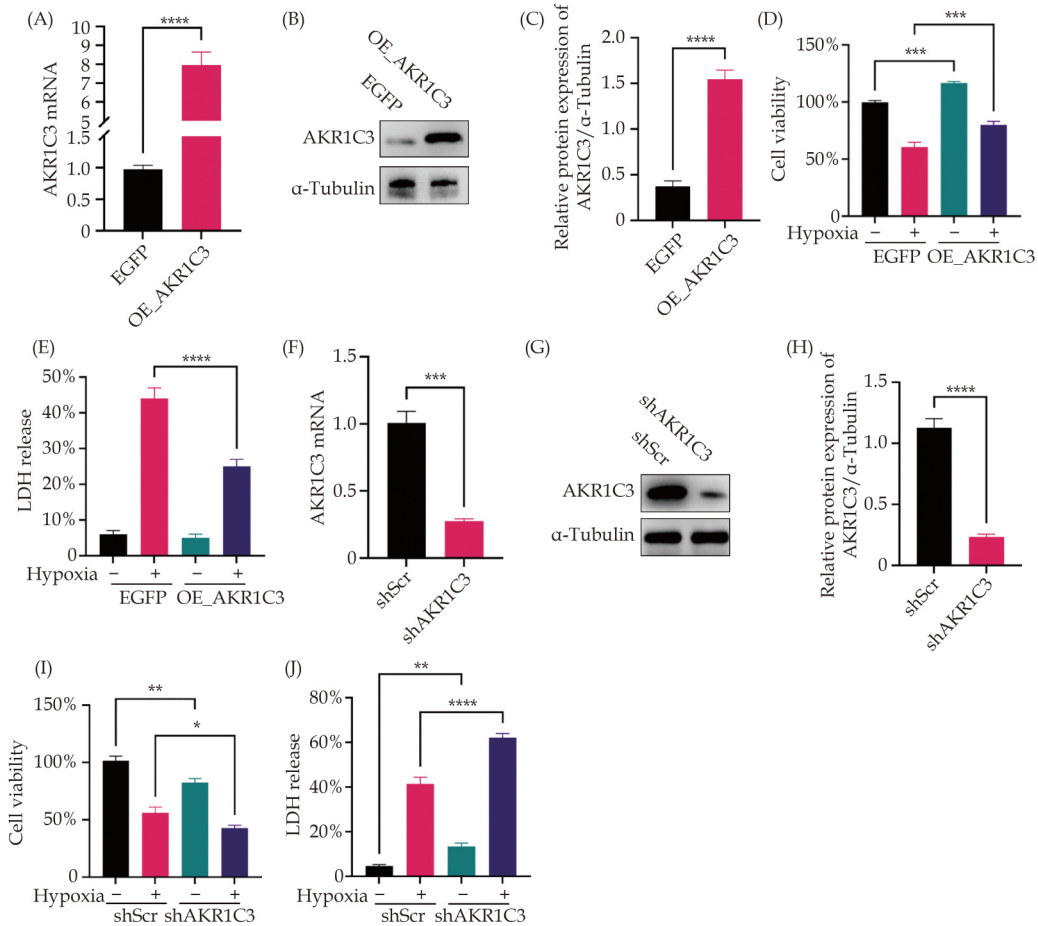

Figure 3 AKR1C3 regulates cell viability in hypoxia-treated H9C2 cells. (A-C): Verification of mRNA and protein levels in H9C2 cells with overexpressed AKR1C3; (D, E): Cell viability and LDH release in H9C2 cells with overexpressed AKR1C3 and the control group after hypoxia treatment. (F-H): Verification of mRNA and protein levels in H9C2 cells with knocked-down AKR1C3; (I, J): Cell viability and LDH release in H9C2 cells with knocked-down AKR1C3 and the control group after hypoxia treatment. $^{*}P < 0.05$, $^{**}P < 0.01$, $^{***}P < 0.001$, $^{****}P < 0.0001$.

oxia group displayed higher cytoplasmic and lower nuclear Nrf2, increased total Keap1, and reduced HO-1 and NQO-1 levels compared to the shScr_Hypoxia group, suggesting that the Keap1-Nrf2-ARE pathway is suppressed (Figure 6O-P).

Keap1-Nrf2-ARE Pathway Regulates Cell Viability and Ferroptosis in Hypoxia-Treated H9C2 Cells

To further explore the role of the Keap1-Nrf2-ARE pathway in regulating ferroptosis in hypoxia-treated H9C2 cells by AKR1C3, the Nrf2 inhibitor ML385 was introduced. The CCK-8 assay showed that combined ML385 treatment reduced cell viability and counteracted the beneficial effects of AKR1C3 overexpression (Figure 7A) while also increasing LDH release (Figure 7B). Furthermore, it resulted in higher Fe^{2+}, BODIPY, and MDA levels alongside a lower GSH/GSSG ratio. Western blot analysis of ferroptosis-related proteins revealed reduced expressions of GPX4 and SLC7A11 (Figure 7C-H). These results reveal that Keap1-Nrf2-ARE pathway inhibition decreases cell viability and increases ferroptosis in hypoxia-treated H9C2 cells.

Lastly, we used (R)-Sulforaphane, an activator of the Keap1-Nrf2-ARE pathway. As shown in Figures 7I and J, hypoxia-treated H9C2 cells with AKR1C3 knockdown showed increased cell viability and reduced LDH release after treatment with (R)-Sulforaphane. In addition, in hypoxia-treated cells, treatment with (R)-Sulforaphane led to lower Fe^{2+}, BODIPY, and MDA levels, an increased GSH/GSSG ratio, along with higher expressions of GPX4 and SLC7A11 (Figures 7K-P). This suggests that under hypoxic conditions, (R)-Sulforaphane can enhance

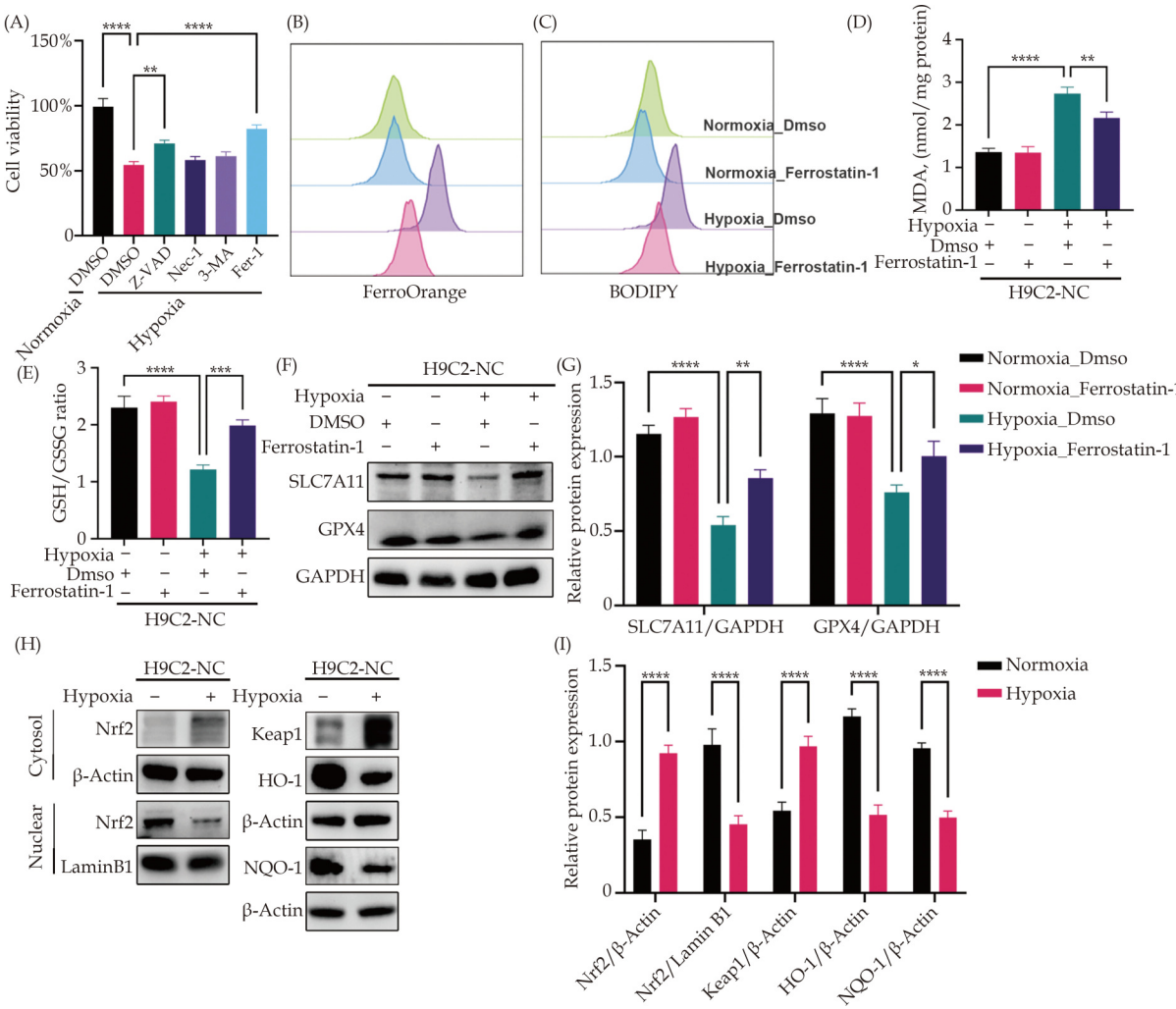

Figure 4 Hypoxia treatment increases ferroptosis and inhibits the Keap1-Nrf2-ARE pathway in H9C2 cells. (A): Tests with various inhibitors suggested that Ferrostatin-1 showed the most substantial recovery effect on H9C2 cell viability after hypoxia; (B-H): Levels of Fe^{2+}, BODIPY, and MDA, the GSH/GSSG ratio, and levels of GPX4 and SLC7A11 in hypoxia-treated H9C2 cells; (H, I): Levels of cytoplasmic Nrf2, nuclear Nrf2, total Keap1, HO-1, and NQO-1 in hypoxia-treated H9C2 cells. BODIPY: boron-dipyrromethane; GPX4: glutathione peroxidase 4; GSH/GSSG: glutathione/glutathione disulfide; HO-1: heme oxygenase; Keap1-Nrf2-ARE: Kelch-like ECH-associated protein 1-nuclear factor erythroid 2-related factor 2-antioxidant response element; MDA: malondialdehyde; NQO-1: nicotinamide adenine dinucleotide phosphate dehydrogenase quinone dehydrogenase; SLC7A11: solute carrier 7A11. $^{*}P < 0.05$, $^{**}P < 0.01$, $^{***}P < 0.001$, $^{****}P < 0.0001$.

cell viability and reduce ferroptosis in AKR1C3-knockdown H9C2 cells. Collectively, these findings suggest that the Keap1-Nrf2-ARE pathway plays a key role in AKR1C3's regulation of cell viability and ferroptosis in hypoxia-treated H9C2 cells.

DISCUSSIONS

This study established an AMI rat model through coronary artery ligation. Myocardial tissue damage was confirmed by echocardiography and HE and Masson staining. RT-qPCR and western blot showed reduced AKR1C3 levels. Subsequently, an *in vitro* AMI model was created using hypoxia-treated H9C2 cells. The results indicated that hypoxia decreased cell viability and reduced mRNA and protein levels of AKR1C3, consistent with the observations in the AMI rat model. Lentiviral transfection was conducted to create cell lines that overexpressed or knocked down AKR1C3 to understand its role in regulating H9C2 cell viability. Overexpressing AKR1C3 increased cell viability after hypoxia compared to the control group, while knocking down

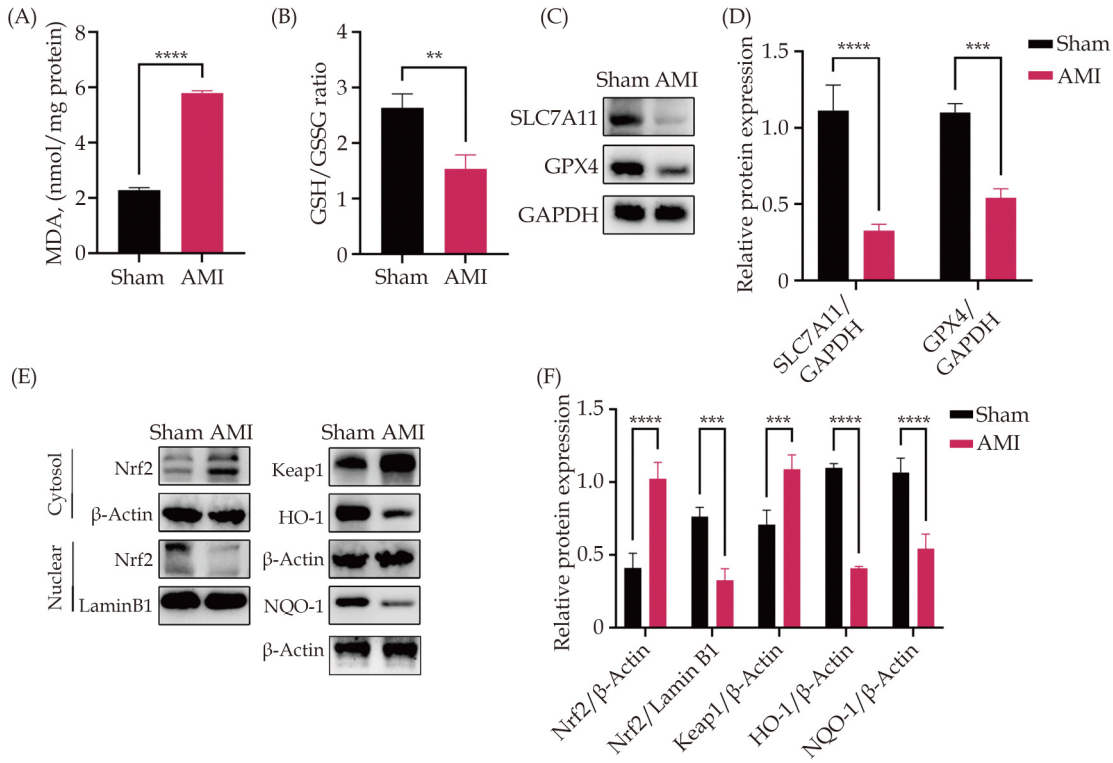

Figure 5 Ferroptosis increases, and the Keap1-Nrf2-ARE pathway is inhibited in rat myocardial tissue after AMI. Comparison between the AMI group and the Sham group for (A-D): Levels of MDA, GSH/GSSG ratio, GPX4, and SLC7A11; (E, F): Levels of cytoplasmic Nrf2, nuclear Nrf2, total Keap1, HO-1, and NQO-1. $^{**}P < 0.01$, $^{***}P < 0.001$, $^{****}P < 0.0001$.

AKR1C3 led to the opposite effect. Next, the types of cell death involved were examined. Of the inhibitors tested, Ferrostatin-1 showed the most significant effect on restoring cell viability. When subjected to hypoxia treatment, H9C2 cells showed escalated levels of Fe^{2+}, BODIPY, and MDA, along with lower GSH/GSSG ratios and reduced expressions of GPX4 and SLC7A11. However, this effect was partially reversed by introducing Ferrostatin-1, suggesting increased ferroptosis. In addition, hypoxia treatment inhibited the Keap1-Nrf2-ARE pathway in H9C2 cells. Overexpression of AKR1C3 reduced ferroptosis and activated this pathway, while AKR1C3 knockdown exhibited the opposite effect. Lastly, inhibiting the Keap1-Nrf2-ARE pathway with ML385 in hypoxia-treated H9C2 cells reduced cell viability

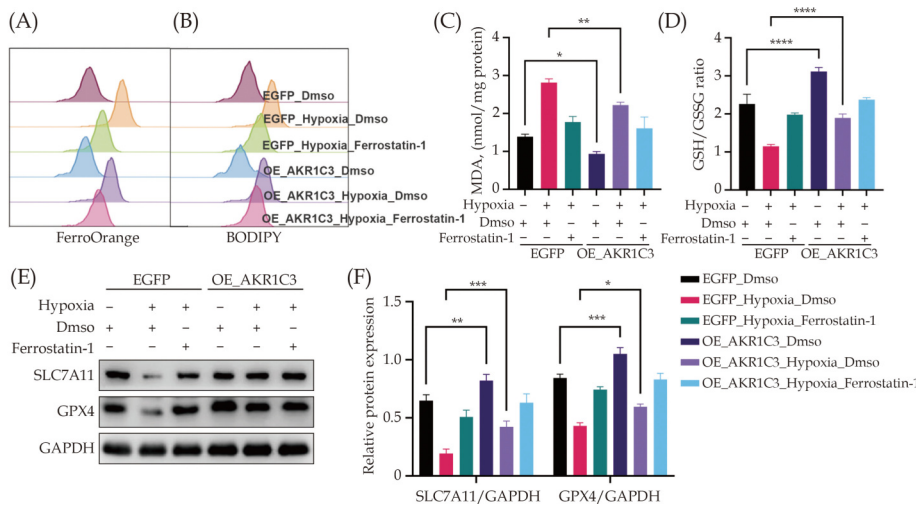

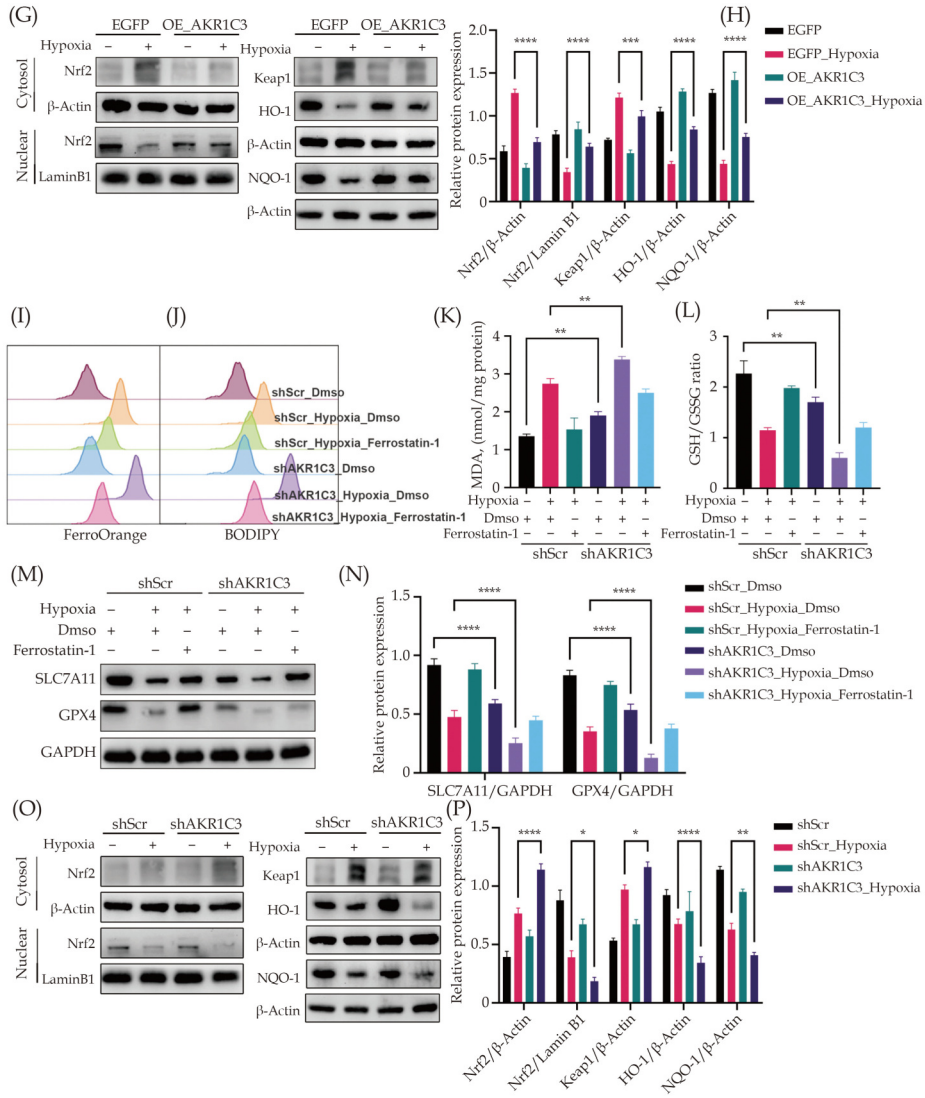

Figure 6 AKR1C3 regulates ferroptosis and the Keap1-Nrf2-ARE pathway in hypoxia-treated H9C2 cells. (A-F): Comparison between H9C2 cells overexpressing AKR1C3 and the control group after hypoxia treatment for Fe^{2+}, BODIPY and MDA levels, the GSH/GSSG ratio, GPX4, and SLC7A11; (G-H): cytoplasmic Nrf2, nuclear Nrf2, and total protein levels of Keap1, HO-1, and NQO-1; Comparison between H9C2 cells knocked-down AKR1C3 and the control group after hypoxia treatment for (I-N): Fe^{2+}, BODIPY and MDA levels, the GSH/GSSG ratio, GPX4, and SLC7A11; (O-P): cytoplasmic Nrf2, nuclear Nrf2, and total protein levels of Keap1, HO-1, and NQO-1. $^{*}P < 0.05$, $^{**}P < 0.01$, $^{***}P < 0.001$, $^{****}P < 0.0001$.

and increased ferroptosis. Conversely, activation with (R)-Sulforaphane produced the opposite effect.

AMI is caused by sudden coronary artery occlusion and poses a significant threat to human health.[11] However, there are currently no drugs that specifically target AMI for treatment or prevention. Therefore, developing effective clinical therapies to mitigate the severe consequences of AMI incurs great clinical importance. Following AMI, oxidative stress is a major cause of cellular damage, and changes in oxidative stress post-AMI can be closely linked to the prognosis following PCI.[23] AKR1C3 is a critical molecule involved in cellular oxidative stress.[9] Research shows that AKR1C3 improves tumor sensitivity to ionizing radiation by regulating oxidative stress levels. Wang, *et al.*[24] reported that high AKR1C3 expressions reduced the levels of cytoplasmic Fe^{2+} and lipid peroxides, suggesting that overexpressing AKR1C3 can inhibit ferroptosis. Lin, *et al.*[25] analyzed the expression of antioxidant-related proteins in smokers and non-smokers using bioinformatics which showed significant upregula-

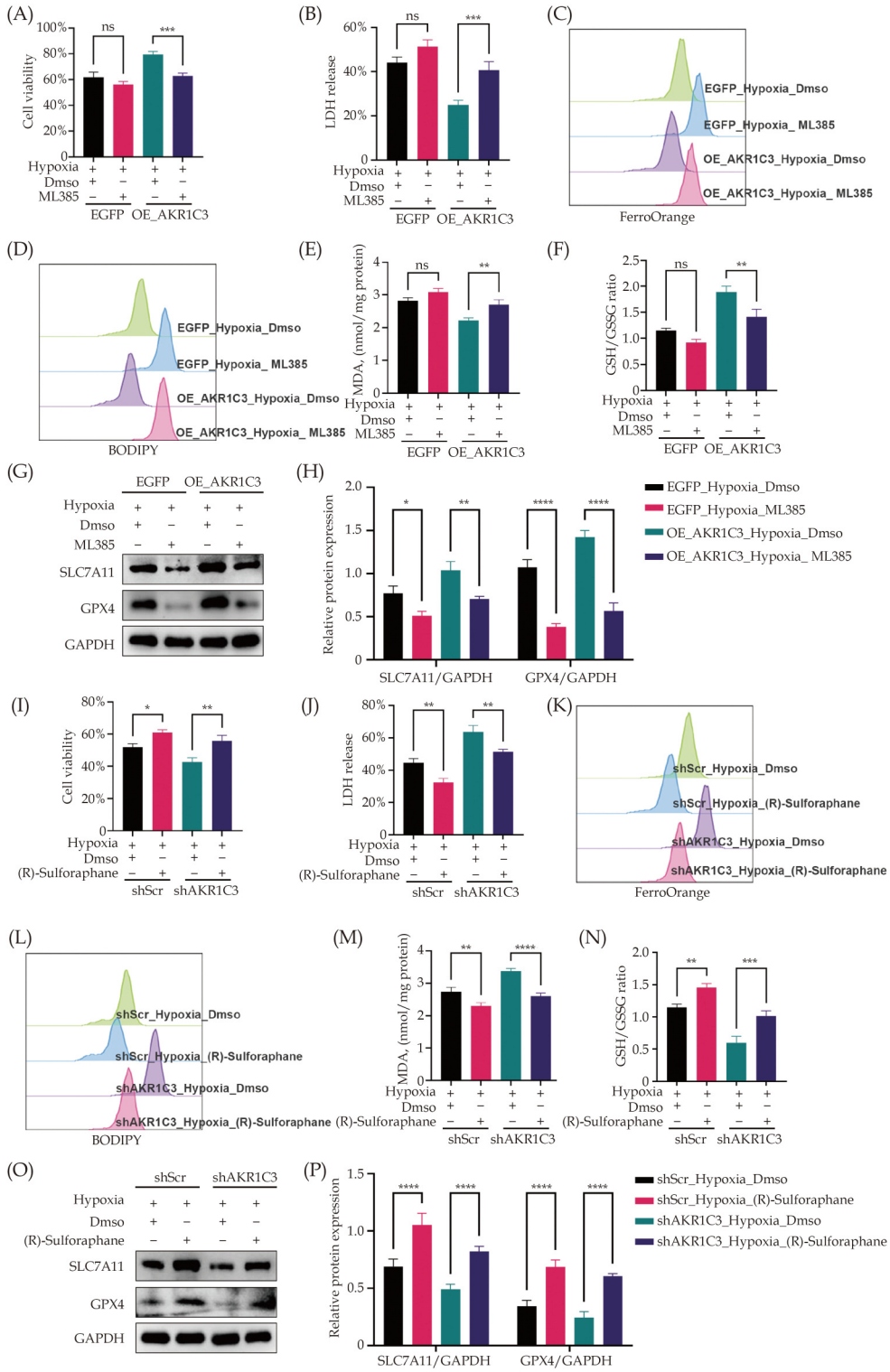

Figure 7 The Keap1-Nrf2-ARE pathway regulates cell viability and ferroptosis in hypoxia-treated H9C2 cells. In H9C2 cells overexpressing AKR1C3, the effects of hypoxia treatment with ML385 results are displayed in (A, B): Cell viability and LDH release; (C-H): Fe^{2+}, BODIPY and MDA levels, the GSH/GSSG ratio, GPX4, and SLC7A11;In H9C2 cells overexpressing AKR1C3, the effects of hypoxia treatment with ML385 results are displayed in (I, J): Cell viability and LDH release; (K-P): Fe^{2+}, BODIPY and MDA levels, the GSH/GSSG ratio, GPX4, and SLC7A11. $^{*}P < 0.05$, $^{**}P < 0.01$, $^{***}P < 0.001$, $^{****}P < 0.0001$.

tion of AKR1C3 in the former. Liang, *et al.* [11] indicated that AKR1C3 could be a potential biomarker for AMI. Our study found that AKR1C3 levels decreased in rats after AMI and in hypoxia-treated H9C2 cells. Overexpressing AKR1C3 improved cell viability after hypoxia while knocking it down had the opposite effect.

Ferroptosis is a form of cell death associated with oxidative stress[12] and plays a significant role in AMI.[13] It is driven by the Fenton reaction, in which excess Fe^{2+} leads to lipid peroxidation, manifested as increased MDA. In addition, the downregulation of SLC7A11 leads to reduced intracellular cystine and GSH depletion, promoting the accumulation of lipid peroxides. This indirectly inhibits GPX4 activity, thereby increasing lipid peroxidation. Ultimately, these factors can collectively contribute to increased ferroptosis. Reducing ferroptosis after AMI is an effective strategy to mitigate myocardial cell damage and improve treatment outcomes.[14] Li, *et al.*[26] found that miR-26b-5p downregulation in plasma exosomes from patients with AMI reduced myocardial cell damage by inhibiting ferroptosis after AMI. Similarly, Liu, *et al.*[27] reported that resveratrol, an antioxidant, induced KAT5 expression, which increased GPX4 levels, thereby inhibiting ferroptosis and, on this basis, mitigating myocardial damage after AMI. Our findings indicate that ferroptosis is increased in hypoxia-treated H9C2 cells, a result also observed in the AMI rat model. In addition, overexpression of AKR1C3 reduces ferroptosis in hypoxia-treated H9C2 cells, while knocking down AKR1C3 increases ferroptosis.

Another finding from our study is that hypoxia-treated H9C2 cells showed decreased nuclear Nrf2, increased cytoplasmic Nrf2, elevated total Keap1, and reduced HO-1 and NQO-1 levels. In addition, we observed similar results in the AMI rat model, suggesting the Keap1-Nrf2-ARE pathway inhibition. As a classic oxidative stress pathway, the Keap1-Nrf2-ARE pathway plays an essential role in the occurrence and progression of ferroptosis and AMI. Yao, *et al.*[28] demonstrated that activating the Nrf2-HO1 pathway inhibited ferroptosis following myocardial ischemia-reperfusion. Wu, *et al.*[29] found that targeting Nrf2 with Ferrostatin-1 to modulate ferroptosis levels was closely related to reduced cell damage after AMI. Furthermore, our study revealed that overexpressing AKR1C3 in H9C2 cells activated the Keap1-Nrf2-ARE pathway after hypoxia, providing a beneficial effect to cells undergoing hypoxic stress. In contrast, knocking down AKR1C3 yielded the opposite results. In addition, combined treatment with ML385 negated the beneficial effects of AKR1C3 overexpression in hypoxia-treated H9C2 cells, reducing cell viability and increasing ferroptosis. Meanwhile, treatment with (R)-Sulforaphane reversed the suppression of the Keap1-Nrf2-ARE pathway caused by AKR1C3 knockdown, resulting in increased cell viability and reduced ferroptosis. These findings suggest that AKR1C3 regulates ferroptosis in hypoxia-treated H9C2 cells through the Keap1-Nrf2-ARE pathway.

This study offers valuable insights into the function of AKR1C3 in AMI rats and hypoxia-treated H9C2 cells. However, it has some limitations. Further clinical studies are needed to validate whether AKR1C3 overexpression can protect against myocardial damage following AMI. Moreover, identifying the downstream molecules of AKR1C3 and exploring the potential mechanisms may yield more comprehensive insights.

In conclusion, this study shows that AKR1C3 levels decrease in rats with AMI and hypoxia-treated H9C2 cells. Overexpressing AKR1C3 increases cell viability in hypoxia-treated H9C2 cells and can inhibit ferroptosis by Keap1-Nrf2-ARE pathway activation, whereas AKR1C3 knockdown exhibits the opposite effect. Regulating the Keap1-Nrf2-ARE pathway can reverse the effects of AKR1C3 knockdown on cell viability and ferroptosis. These results suggest that AKR1C3 may serve as a promising target for mitigating cell damage after AMI, with potential applications in clinical settings.

DISCLOSURE

Conflicts of Interest

None.

Fundings

This study was supported by the Traditional Chinese Medicine Bureau of Guangdong Province, Guangzhou (grant No. 20231321) and by the Clinical research initiation program project from Shunde

Hospital, Southern Medical University, Foshan (grant No. CRSP2022004).

REFERENCES

[1] Bhatt DL, Lopes RD, Harrington RA. Diagnosis and treatment of acute coronary syndromes: A Review. *JAMA* 2022; 327: 662−675.

[2] Sarfo FS, Nichols M, Opare-Addo PA, *et al*. Polypill programs to prevent stroke and cut costs in low income countries: moving from clinical efficacy to pragmatic implementation. *Stroke* 2023; 54: 407−414.

[3] Bugger H, Pfeil. Mitochondrial ROS in myocardial ischemia reperfusion and remodeling. *Biochim Biophys Acta Mol Basis Dis* 2020; 1866: 165768.

[4] Del Re DP, Amgalan D, Linkermann A, *et al*. Fundamental Mechanisms of Regulated Cell Death and Implications for Heart Disease. *Physiol Rev* 2019; 99: 1765−1817.

[5] Xu Y, Dong Z, Zhang R, *et al*. Sonodynamic therapy reduces cardiomyocyte apoptosis through autophagy activated by reactive oxygen species in myocardial infarction. *Free Radic Biol Med* 2023; 195: 36-46.

[6] Lu X, Yang B, Qi R, *et al*. Targeting WWP1 ameliorates cardiac ischemic injury by suppressing KLF15-ubiquitination mediated myocardial inflammation. *Theranostics* 2023; 13: 417−437.

[7] Heusch G, Andreadou I, Bell R, *et al*. Health position paper and redox perspectives on reactive oxygen species as signals and targets of cardioprotection. *Redox Biol* 2023; 67: 102894.

[8] Teixeira RB, Pfeiffer M, Zhang P, *et al*. Reduction in mitochondrial ROS improves oxidative phosphorylation and provides resilience to coronary endothelium in non-reperfused myocardial infarction. *Basic Res Cardiol* 2023; 118: 3.

[9] Penning TM. AKR1C3 (type 5 17β-hydroxysteroid dehydrogenase/prostaglandin F synthase): Roles in malignancy and endocrine disorders. *Mol Cell Endocrinol* 2019; 489: 82-91.

[10] Huang W, Wang Y, Huang W. Mangiferin alleviates 6-OHDA-induced Parkinson's disease by inhibiting AKR-1C3 to activate Wnt signaling pathway. *Neurosci Lett* 2024; 821: 137608.

[11] Liang J, Cao Y, He M, *et al*. AKR1C3 and Its Transcription Factor HOXB4 Are Promising Diagnostic Biomarkers for Acute Myocardial Infarction. *Front Cardiovasc Med* 2021; 8: 694238.

[12] Song S, Su Z, Kon N, *et al*. ALOX5-mediated ferroptosis acts as a distinct cell death pathway upon oxidative stress in Huntington's disease. *Genes Dev* 2023; 37: 204−217.

[13] Song Y, Wang B, Zhu X, *et al*. Human umbilical cord blood-derived MSCs exosome attenuate myocardial injury by inhibiting ferroptosis in acute myocardial infarction mice. *Cell Biol Toxicol* 2021; 37: 51−64.

[14] Sun Q, Ma H, Zhang J, *et al*. A self-sustaining antioxidant strategy for effective treatment of myocardial infarction. *Adv Sci (Weinh)* 2023; 10: e2204999.

[15] Jiang Y, Qiao Y, He D, *et al*. Adaptor protein HIP-55-mediated signalosome protects against ferroptosis in myocardial infarction. *Cell Death Differ* 2023; 30: 825-838.

[16] Yu Q, Zhang N, Gan X, *et al*. EGCG attenuated acute myocardial infarction by inhibiting ferroptosis via miR-450b-5p/ACSL4 axis. *Phytomedicine* 2023; 119: 154999.

[17] Suzuki T, Yamamoto M. Molecular basis of the Keap1-Nrf2 system. *Free Radic Biol Med*. 2015; 88(Pt B): 93-100.

[18] Yao Y, Li P, Jiang S, *et al*. A Mechanism Study on the Antioxidant Pathway of Keap1-Nrf2-ARE Inhibiting Ferroptosis in Dopaminergic Neurons. *Curr Mol Med* 2024; e030124225217.

[19] Zhang X, Yu Y, Lei H, *et al*. The Nrf-2/HO-1 signaling axis: a ray of hope in cardiovascular diseases. *Cardiol Res Pract* 2020; 5695723.

[20] Liu J, Li Y, Wu S, *et al*. Hyperbaric oxygen upregulates Mst1 to activate Keap1/Nrf2/HO-1 pathway resisting oxidative stress in a rat model of acute myocardial infarction. *Mol Biotechnol* 2024. DOI: 10.1007/s12033-024-01050-8. Published online first: Feb 23, 2024.

[21] Ma Y, Pan C, Tang X, *et al*. MicroRNA-200a represses myocardial infarction-related cell death and inflammation by targeting the Keap1/Nrf2 and β-catenin pathways. *Hellenic J Cardiol* 2021; 62: 139−148.

[22] Canning P, Sorrell FJ, Bullock AN. Structural basis of Keap1 interactions with Nrf2. *Free Radic Biol Med* 2015; 88(Pt B): 101-107.

[23] de Koning MLY, Al Ali L, Bourgonje AR, *et al*. Associations of systemic oxidative stress with functional outcomes after ST-segment elevation myocardial infarction. *Int J Cardiol* 2023; 391: 131214.

[24] Wang Y, Fan J, Tong Y, *et al*. Bioinformatics analysis of ferroptosis-related gene AKR1C3 as a potential biomarker of asthma and its identification in BEAS-2B cells. *Comput Biol Med* 2023; 158: 106740.

[25] Lin Z, Xu Y, Guan L, *et al*. Seven ferroptosis-specific expressed genes are considered as potential biomarkers for the diagnosis and treatment of cigarette smoke-induced chronic obstructive pulmonary disease. *Ann Transl Med* 2022; 10: 331.

[26] Li H, Ding J, Liu W, *et al*. Plasma exosomes from patients with acute myocardial infarction alleviate myocardial injury by inhibiting ferroptosis through miR-26b-5p/SLC7A11 axis. *Life Sci* 2023; 322: 121649.

[27] Liu J, Zhang M, Qin C, *et al*. Resveratrol Attenuate Myocardial Injury by Inhibiting Ferroptosis *Via* Inducing KAT5/GPX4 in Myocardial Infarction. *Front Pharmacol* 2022; 13: 906073.

[28] Yao H, Xie Q, He Q, *et al*. Pretreatment with Panaxatriol Saponin Attenuates Mitochondrial Apoptosis and Oxidative Stress to Facilitate Treatment of Myocardial Ischemia-Reperfusion Injury via the Regulation of Keap1/Nrf2 Activity. *Oxid Med Cell Longev* 2022; 2022: 9626703.
[29] Wu YT, Zhang GY, Hua Y, *et al*. Ferrostatin-1 suppresses cardiomyocyte ferroptosis after myocardial infarction by activating Nrf2 signaling. *J Pharm Pharmacol* 2023; 75: 1467−1477.

Please cite this article as: MIAO W, HU YZ. Aldo-Keto reductase 1C3 reduces myocardial cell damage after acute myocardial infarction by activating the Kelch-like ECH-associated protein 1-nuclear factor erythroid 2-related factor 2-antioxidant response element pathway to inhibit ferroptosis. *J Geriatr Cardiol* 2024; 21(9): 899−912. DOI: 10.26599/1671-5411.2024.09.001